

LETTER • OPEN ACCESS

Direct thermal imaging of the influence of a transition metal dichalcogenide interlayer on a spin-current injection in a Pt/Y₃Fe₅O₁₂ heterostructure

To cite this article: Shun-ichi Takano *et al* 2026 *Jpn. J. Appl. Phys.* **65** 080907

View the [article online](#) for updates and enhancements.

You may also like

- [Spin Peltier effect and its length scale in Pt/YIG system at high temperatures](#)
Atsushi Takahagi, Takamasa Hirai, Ryo Iguchi *et al.*
- [Charge-current angle and frequency dependences of the spin Peltier effect induced by the spin Hall effect](#)
Ryo Iguchi and Ken-ichi Uchida
- [Enhanced thermo-spin effects in iron-oxide/metal multilayers](#)
R Ramos, I Lucas, P A Algarabel *et al.*



Direct thermal imaging of the influence of a transition metal dichalcogenide interlayer on a spin-current injection in a Pt/Y₃Fe₅O₁₂ heterostructure

Shun-ichi Takano^{1,2} , Wenjin Zhang³ , Yui Tamogami^{3,4} , Takamasa Hirai² , Shunsuke Mori^{1,2} , Yasumitsu Miyata^{3,4} , Ken-ichi Uchida^{1,2*} , and Yusuke Nakanishi^{1,2*}

¹Department of Advanced Materials Science, Graduate School of Frontier Sciences, The University of Tokyo, Kashiwa 277-8561, Japan

²Research Center for Magnetic and Spintronic Materials, National Institute for Materials Science, Tsukuba 305-0047, Japan

³Research Center for Materials Nanoarchitectonics, National Institute for Materials Science, Tsukuba 305-0044, Japan

⁴Department of Physics, Tokyo Metropolitan University, Hachioji 192-0397, Japan

*E-mail: UCHIDA.Kenichi@nims.go.jp; naka24ysk@edu.k.u-tokyo.ac.jp

Received March 18, 2026; revised April 13, 2026; accepted April 20, 2026; published online May 5, 2026

The spin Peltier effect (SPE) in Pt/WSe₂/Y₃Fe₅O₁₂ (YIG) and Pt/WS₂/YIG heterostructures is investigated using lock-in thermography. Since inserting atomically thin transition metal dichalcogenides (TMDs), such as WSe₂, between Pt and YIG is known to enhance the voltage induced by the spin Seebeck effect, similar enhancement is expected for SPE. Contrary to this expectation, the SPE-induced temperature modulation is strongly suppressed in the TMD-inserted regions compared with bare Pt/YIG regions. Raman spectroscopy reveals sputtering-induced structural degradation of WSe₂, hindering spin-current injection into YIG. These results highlight the sensitivity of spin-current transport to interface quality in spin-caloritronic devices incorporating atomically thin TMDs. © 2026 The Japan Society of Applied Physics. All rights, including for text and data mining, AI training, and similar technologies, are reserved.

The integration of thermoelectric conversion into spintronics has led to the development of spin caloritronics,^{1–3)} which provides novel energy conversion principles. The representative phenomena of spin-current transport in spin caloritronics include the spin Seebeck effect (SSE)^{4–6)} and the spin Peltier effect (SPE).^{7,8)} SSE and SPE enable interconversion between heat and spin currents in magnetic materials, functioning as a transverse thermoelectric conversion through the spin–orbit coupling in metals attached to the magnetic materials.^{9,10)} SSE and SPE have been extensively investigated in paramagnet/ferromagnet (or ferrimagnet) junctions such as Pt/Y₃Fe₅O₁₂ (YIG),^{7,8,11–13)} where the strong spin–orbit coupling in Pt enables interconversion between charge and spin currents via the (inverse) spin Hall effect.^{14–18)} The output voltage induced by SSE and temperature modulation induced by SPE are much smaller than those of the conventional Seebeck and Peltier effects. However, SSE and SPE exhibit unique functionalities including the transverse thermoelectric conversion using insulators owing to their magnon origin.

SSE and SPE are strongly influenced by the efficiency of spin-angular-momentum transfer across paramagnet/ferromagnet interfaces,^{19–21)} which is quantified by the spin-mixing conductance.^{22,23)} Recently, the inverse spin Hall voltage induced by SSE was found to be enhanced by insertion of atomically thin transition metal dichalcogenides (TMDs)^{24,25)} into the paramagnet/ferromagnet interfaces, e.g., in Pt/WSe₂/YIG heterostructures [Fig. 1(a)].²⁶⁾ However, the influence of the TMD-inserted interfaces on spin-current transport remains unclear since SSE signals reflect average information of the entire sample and is determined by multiple parameters including the spin mixing conductance and spin Hall angle. To investigate the effect of TMDs on SSE or SPE signals, spatially resolved measurements are useful.

In this letter, we investigate SPE in Pt/WSe₂/YIG and Pt/WS₂/YIG heterostructures through active thermal imaging

measurements based on lock-in thermography (LIT).⁸⁾ We first focus on Pt/WSe₂/YIG, where enhanced SPE-induced temperature modulation is expected to occur owing to the reciprocity between SSE and SPE. The LIT measurements show that, contrary to the expectation, SPE-induced signals are suppressed in the WSe₂-inserted regions, suggesting suppression of the spin-current injection from Pt into YIG. Raman spectroscopy shows that the inserted WSe₂ layer may be damaged during Pt sputtering. The same behaviors were observed in Pt/WS₂/YIG. These observations indicate that spin transport across the Pt/YIG interface is strongly affected by the damage of atomically thin TMD interlayers, highlighting the importance of careful interface engineering in the integration of atomically thin materials into spin-caloritronic devices.

Our Pt/WSe₂/YIG sample was prepared as follows. WSe₂ flakes were synthesized by salt-assisted chemical vapor deposition (CVD). An optical micrograph shows atomically flat triangular flakes [Fig. 2(a)], characteristic of CVD-grown monolayer WSe₂ with zigzag edges.²⁷⁾ The as-grown flakes were characterized by Raman spectroscopy and atomic force microscopy (AFM). The Raman spectrum exhibits a characteristic peak at ~250 cm^{−1}, corresponding to E' and A₁' modes of WSe₂, respectively [Fig. 2(b)].²⁸⁾ An AFM topographic image [Fig. 2(c)] and its line profile [Fig. 2(d)] reveal a thickness of the CVD-grown WSe₂ to be ~0.7 nm, consistent with monolayer WSe₂. The as-grown WSe₂ flakes were subsequently transferred onto single-crystalline YIG, grown on a single-crystalline Gd₃Ga₅O₁₂ (111) substrate by a liquid phase epitaxy method, using a poly(methyl methacrylate)-assisted wet-transfer process. The thickness of YIG was 17 μm, much larger than the characteristic length of SPE,^{29,30)} and the substrate was cut into a rectangular shape with a size of 2 mm in width and 7 mm in length. Finally, a 5-nm-thick Pt layer was deposited on the YIG substrate with WSe₂ flakes at room temperature by RF magnetron sputtering with a power of 50 W under an



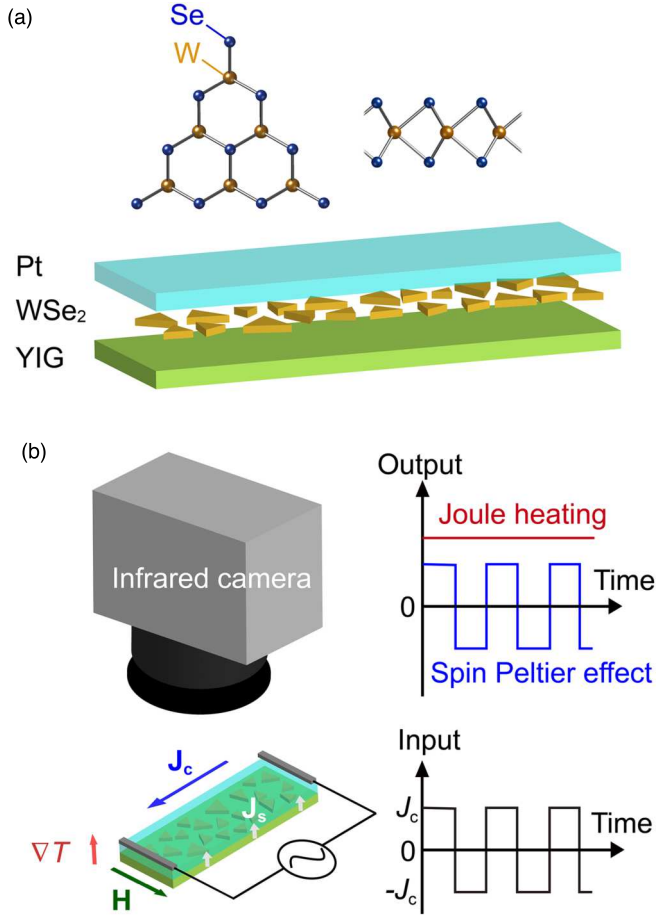


Fig. 1. (a) Schematic of the crystal structure of WSe₂ and the Pt/WSe₂/YIG heterostructure. (b) Schematic of SPE measurements using LIT. J_c , J_s , H , and ∇T denote the square-wave-modulated AC charge current with amplitude J_c , spatial direction of the spin current, magnetic field, and temperature gradient, respectively.

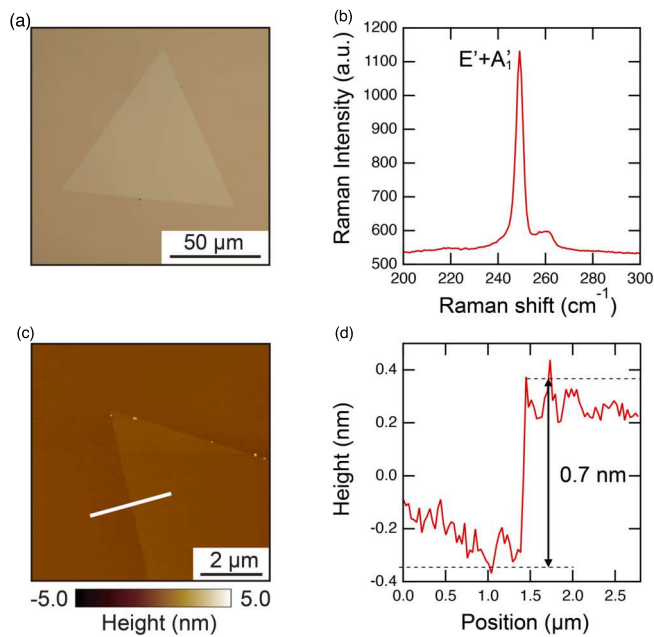


Fig. 2. (a) Optical microscope image of an as-grown WSe₂ flake. (b) Raman spectrum of WSe₂. (c) AFM image of WSe₂. (d) Height profile along the white line in (c).

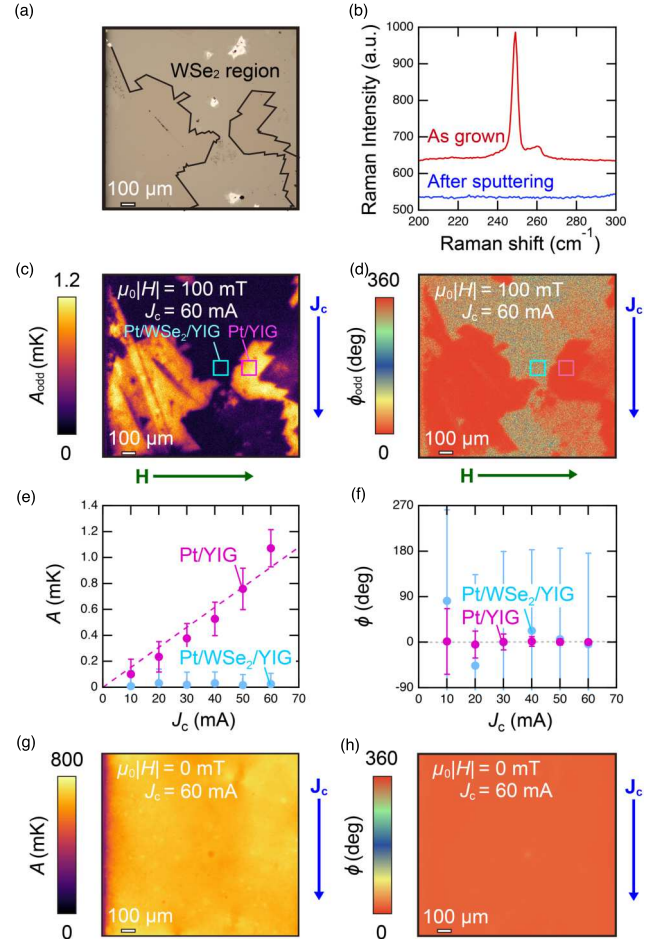


Fig. 3. (a) Optical microscope image of the Pt/WSe₂/YIG sample corresponding to the LIT measurement region. (b) Raman spectra of WSe₂ before and after Pt sputtering. (c), (d) H -odd-dependent components of the A_{odd} and ϕ_{odd} images for the Pt/WSe₂/YIG sample at $J_c = 60$ mA, $f = 5$ Hz, and $\mu_0 H l = 100$ mT, where μ_0 is the vacuum permeability. (e), (f) J_c dependence of the A_{odd} and ϕ_{odd} signals for the Pt/YIG (Pt/WSe₂/YIG) region, marked with a pink (light blue) square in (c) and (d), at $f = 5$ Hz and $\mu_0 H l = 100$ mT. The dotted line in (e) represents a linear fit. (g), (h) A and ϕ images at $J_c = 60$ mA, $f = 25$ Hz, and $\mu_0 H l = 0$ mT.

Ar pressure of 0.3 Pa. As shown in an optical micrograph in Fig. 3(a), the transferred WSe₂ flakes result in the formation of a WSe₂ interlayer only on certain areas of YIG, where the presence of WSe₂ is confirmed by the Raman spectrum in Fig. 3(b). This allows for simultaneous comparison of SPE signals within a single sample between regions with and without the interlayer.

Applying a charge current J_c to the Pt layer of the Pt/WSe₂/YIG sample generates a spin current perpendicular to the interface due to the spin Hall effect [Fig. 1(b)]. This spin current is injected into the YIG layer in areas where WSe₂ is absent. In areas where WSe₂ is present, the spin-current injection is affected by the interlayer. The spin current injected into the YIG layer generates a heat current near the interface via SPE, resulting in a temperature change on the sample surface that is linearly proportional to the applied charge current. This process occurs when the magnetization of YIG is in-plane and perpendicular to J_c .⁸⁾

The spatial distribution of the SPE-induced temperature modulation in the Pt/WSe₂/YIG sample was measured using LIT under an in-plane magnetic field H (with the magnitude

© 2026 The Japan Society of Applied Physics. All rights, including for text and data mining, AI training, and similar technologies, are reserved.

H) [Fig. 1(b)]. During the LIT measurements, a square-wave-modulated AC charge current with the amplitude J_c and frequency f was applied to the Pt layer in the direction perpendicular to \mathbf{H} and the first harmonic response of the detected signals was decomposed into lock-in amplitude A and phase ϕ images by Fourier analysis. When a charge current with zero DC offset is applied, SPE-induced signals ($\propto J_c^2$) can be detected separately from Joule-heating contributions ($\propto J_c^2$).⁸⁾ In contrast, applying an ON-OFF-modulated charge current, i.e., the square-wave-modulated AC current with a finite DC offset, produces Joule-heating-induced signals, which are utilized to evaluate the spatial distribution of the charge current density (note that the contribution of SPE in this measurement condition is negligibly small compared to Joule-heating-induced signals). Since the SPE-induced signals exhibit an antisymmetric dependence on H , the odd components of the LIT amplitude and phase were calculated from raw LIT images measured under a positive or negative field as: $A_{\text{odd}} = [A(+H)e^{-i\phi(+H)} - A(-H)e^{-i\phi(-H)}]/2$ and $\phi_{\text{odd}} = -\arg[A(+H)e^{-i\phi(+H)} - A(-H)e^{-i\phi(-H)}]$. By doing so, we can separate the H -independent Peltier signals at the boundaries between areas with and without WSe_2 . For the LIT measurements, insulating black ink was coated on the sample surface to obtain high (>0.94) and uniform infrared emissivity.

Figures 3(c) and 3(d) display the A_{odd} and ϕ_{odd} images for the Pt/ WSe_2 /YIG sample, measured at $J_c = 60$ mA, $f = 5.0$ Hz, and $\mu_0 H = 100$ mT, where μ_0 denotes the vacuum permeability and the region of interest corresponds to the area shown the optical micrograph in Fig. 3(a). At this magnetic field, the magnetization of the YIG layer is uniformly aligned perpendicular to the \mathbf{J}_c direction, satisfying the symmetry required for SPE signals to manifest.⁸⁾ In the Pt/YIG region without the WSe_2 interlayer, clear SPE-induced signals were observed, where the sign and magnitude of the temperature modulation are consistent with the results in Ref. 31. The magnitude of the A_{odd} signals was proportional to J_c [Fig. 3(e)], while $\phi_{\text{odd}} \sim 0^\circ$ remained unchanged as a function of J_c [Fig. 3(f)]. In contrast, as shown in Figs. 3(c)–3(f), tiny A_{odd} and undefined ϕ_{odd} signals appear in the Pt/ WSe_2 /YIG region, indicating the disappearance of SPE-induced temperature modulation (note that, at a small magnetic field of 100 mT, the contribution from the ordinary Ettingshausen effect in the Pt layer is negligibly small). The signals were reduced in all the WSe_2 -inserted areas, irrespective of the WSe_2 thickness. The averaged magnitude of the A_{odd}/J_c signal at $\mu_0 H = 100$ mT for the regions with and without the WSe_2 interlayers was estimated to be $0.04 \times 10^{-13} \text{ K m}^2 \text{ A}^{-1}$ and $1.79 \times 10^{-13} \text{ K m}^2 \text{ A}^{-1}$, respectively.

The non-uniform SPE signal is not due to non-uniform charge-current distribution in the Pt layer. To verify the current distribution within the sample, the Joule-heating signal was measured using LIT at a high f value. Increasing f suppresses the broadening of temperature changes caused by thermal diffusion, enabling visualization of the charge current path. Figures 3(g) and 3(h) show the A and ϕ images for the same Pt/ WSe_2 /YIG sample, measured at $J_c = 60$ mA and $f = 25.0$ Hz in the absence of a magnetic field. The Joule-heating signals were observed to be nearly

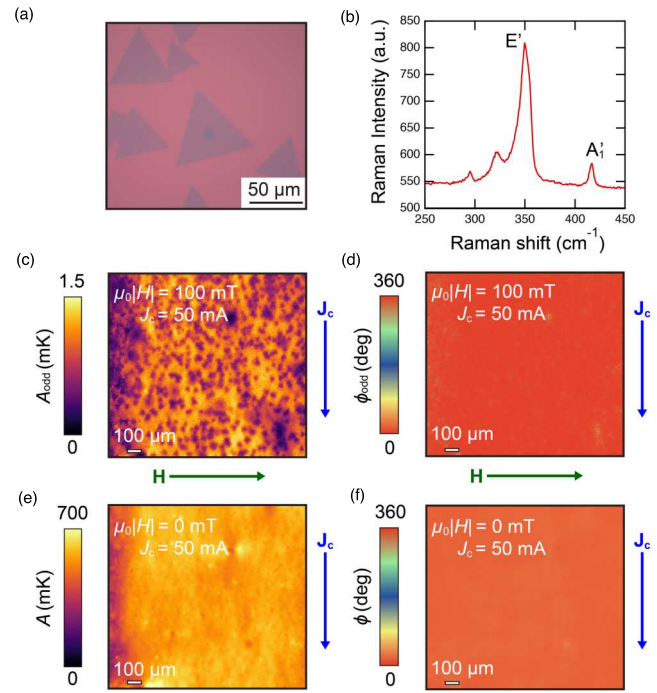


Fig. 4. (a) Optical microscope image of as-grown WS_2 . (b) Raman spectrum of as-grown WS_2 . (c), (d) H -odd-dependent components of the A_{odd} and ϕ_{odd} images for the Pt/ WS_2 /YIG sample at $J_c = 50$ mA, $f = 5$ Hz, and $\mu_0 H = 100$ mT. (e), (f) A and ϕ images at $J_c = 50$ mA, $f = 25$ Hz, and $\mu_0 H = 0$ mT.

uniform across the entire area, indicating the uniform charge-current distribution.

To further confirm the effect of TMDs on spin-current transport, we performed SPE measurements on WS_2 -inserted Pt/YIG heterostructures. First-principles calculations have shown that WSe_2 and WS_2 possess spin-orbit interactions of comparable strength.^{32,33)} In addition, inserting WS_2 between Pt and permalloy was shown to enhance the inverse spin Hall voltage due to thermally induced spin currents.³⁴⁾ Therefore, WSe_2 and WS_2 are expected to exert similar effects on SSE and SPE as interlayers, but their insertion into Pt/YIG systems and SPE measurements have not been reported. Figure 4 presents the measurement results for the Pt/ WS_2 /YIG sample. The triangular shape observed in the optical micrograph [Fig. 4(a)] and the characteristic Raman peaks measured before forming the Pt layer [Fig. 4(b)] confirm the high crystallinity of CVD-grown WS_2 . As shown in Figs. 4(c) and 4(d), the SPE-induced signals were markedly suppressed in the dispersed WS_2 regions (dark spots), similar to the behavior observed in Pt/ WSe_2 /YIG. We also confirmed the uniform current distribution in the Pt/ WS_2 /YIG sample [Figs. 4(e) and 4(f)].

In our experiments, the SPE-induced signals were significantly suppressed in the TMD-inserted regions. This is inconsistent with the previous studies reporting an increase in SSE-induced voltage due to TMD insertion.²⁶⁾ One possible origin of the suppression of the SPE-induced signals in our samples is the formation of interfacial alloy layers at the Pt/TMD interfaces. Although metals deposited on TMDs are generally separated by a van der Waals gap, density functional theory calculations have suggested that certain metals can form covalent bonds with TMDs,³⁵⁾ such as Pd on

WSe₂.³⁶⁾ During sputter deposition, the collision of high-energy atoms onto the TMD surface can induce structural damage^{37–39)} and promote the formation of covalent metal–chalcogen bonds. For WSe₂, Nakajima et al. reported the formation of a metallic alloy layer composed of WO_x, SeO_x, and PtSe_x at the interface between sputtered Pt and WSe₂.⁴⁰⁾ In fact, the Raman peaks characteristic of WSe₂ disappeared after Pt deposition in our samples, suggesting significant damage or structural modification of WSe₂ during sputtering [Fig. 3(b)]. We repeated experiments while decreasing the DC power during sputter deposition to 20 W, but the results remained unchanged. However, considering the uniform charge-current distribution in our samples, the formation of alloy layers may occur only near the interfaces and not affect the electrical resistivity and spin Hall effect within the bulk of the Pt layer. Therefore, we conclude that the formation of the alloy layers significantly reduces the spin injection efficiency at the interfaces,^{41,42)} leading to a reduction in the SPE-induced signals. Although Pt was sputtered also in Ref. 26, the degree of damage to WSe₂ and structure and composition of the alloys formed near the Pt/WSe₂ interface may depend on deposition conditions, such as the sputtering power and target–substrate distance (note that the sputtering power is not provided in Ref. 26). Even with the same method, such variations may account for the discrepancy between the present results and the results in Ref. 26. Since materials with strong spin–orbit coupling, such as Pt, are typically deposited by high-energy sputtering due to their high melting points, low-damage deposition processes are required to preserve the structural integrity of TMDs and ensure efficient interfacial spin transport.

In conclusion, we observed significant suppression of the SPE-induced temperature modulation signals in the Pt/WSe₂/YIG and Pt/WS₂/YIG heterostructures by the LIT technique. Raman spectroscopy indicates that WSe₂ undergoes sputtering-induced damage, which hinders spin-current injection from Pt to YIG. Our results highlight the necessity of low-energy deposition processes for integrating TMDs into spin-caloritronic devices.

Acknowledgments The authors thank T. Endo and M. Isomura for the technical support and T. Kikkawa and S.-K. Lee for the valuable discussions. This work was supported by PRESTO “Nano Materials for New Principle Devices” (JPMJPR23H5), CREST “Nano-Material Semiconductors” (JPMJCR23A4), FOREST (JPMJFR213X), and ERATO “Magnetic Thermal Management Materials Project” (JPMJER2201) from JST, Japan; Grant-in-Aid for Scientific Research (S) (22H04965, 22H04957, 24H00044), Grant-in-Aid for Transformative Research Areas (A) (21H05232, 21H05234), Grant-in-Aid for Scientific Research (B) (23K26500), and Grant-in-Aid for Early-Career Scientists (25K17940) from JSPS KAKENHI, Japan; Noguchi Shitagau Research (NJ202408); and NIMS Joint Research Hub Program. MANA is supported by the World Premier International Research Center Initiative (WPI), MEXT, Japan.

ORCID iDs Shun-ichi Takano <https://orcid.org/0009-0000-4654-2700>
 Wenjin Zhang <https://orcid.org/0000-0002-3803-4770>
 Yui Tamogami <https://orcid.org/0009-0000-8573-940X>
 Takamasa Hirai <https://orcid.org/0000-0002-5577-8018>
 Shunsuke Mori <https://orcid.org/0000-0002-1193-4322>
 Yasumitsu Miyata <https://orcid.org/0000-0002-9733-5119>
 Ken-ichi Uchida <https://orcid.org/0000-0001-7680-3051>
 Yusuke Nakanishi <https://orcid.org/0000-0001-8782-9556>

- 1) G. E. W. Bauer, E. Saitoh, and B. J. van Wees, *Nat. Mater.* **11**, 391 (2012).
- 2) S. R. Boona, R. C. Myers, and J. P. Heremans, *Energy Environ. Sci.* **7**, 885 (2014).
- 3) K. Uchida, *Proc. Jpn. Acad. Ser. B* **97**, 69 (2021).
- 4) K. Uchida, S. Takahashi, K. Harii, J. Ieda, W. Koshibae, K. Ando, S. Maekawa, and E. Saitoh, *Nature* **455**, 778 (2008).
- 5) C. M. Jaworski, J. Yang, S. Mack, D. D. Awschalom, J. P. Heremans, and R. C. Myers, *Nat. Mater.* **9**, 898 (2010).
- 6) K. Uchida et al., *Nat. Mater.* **9**, 894 (2010).
- 7) J. Flipse, F. K. Dejene, D. Wagenaar, G. E. W. Bauer, J. B. Youssef, and B. J. Van Wees, *Phys. Rev. Lett.* **113**, 027601 (2014).
- 8) S. Daimon, R. Iguchi, T. Hioki, E. Saitoh, and K. Uchida, *Nat. Commun.* **7**, 13754 (2016).
- 9) K. Uchida and J. P. Heremans, *Joule* **6**, 2240 (2022).
- 10) H. Adachi, F. Ando, T. Hirai, R. Modak, M. A. Grayson, and K. Uchida, *Appl. Phys. Express* **18**, 090101 (2025).
- 11) K. Uchida, H. Adachi, T. Ota, H. Nakayama, S. Maekawa, and E. Saitoh, *Appl. Phys. Lett.* **97**, 172505 (2010).
- 12) H. Jin, S. R. Boona, Z. Yang, R. C. Myers, and J. P. Heremans, *Phys. Rev. B* **92**, 054436 (2015).
- 13) A. Kehlberger et al., *Phys. Rev. Lett.* **115**, 096602 (2015).
- 14) Y. K. Kato, R. C. Myers, A. C. Gossard, and D. D. Awschalom, *Science* **306**, 1910 (2004).
- 15) E. Saitoh, M. Ueda, H. Miyajima, and G. Tatara, *Appl. Phys. Lett.* **88**, 182509 (2006).
- 16) S. O. Valenzuela and M. Tinkham, *Nature* **442**, 176 (2006).
- 17) A. Hoffmann, *IEEE Trans. Magn.* **49**, 5172 (2013).
- 18) J. Sinova, S. O. Valenzuela, J. Wunderlich, C. H. Back, and T. Jungwirth, *Rev. Mod. Phys.* **87**, 1213 (2015).
- 19) P. Deorani and H. Yang, *Appl. Phys. Lett.* **103**, 232408 (2013).
- 20) D. Kikuchi, M. Ishida, K. Uchida, Z. Qiu, T. Murakami, and E. Saitoh, *Appl. Phys. Lett.* **106**, 082401 (2015).
- 21) H. Yuasa, K. Tamae, and N. Onizuka, *AIP Adv.* **7**, 055928 (2017).
- 22) J. Xiao, G. E. W. Bauer, K. Uchida, E. Saitoh, and S. Maekawa, *Phys. Rev. B* **81**, 214418 (2010).
- 23) H. Adachi, J. Ohe, S. Takahashi, and S. Maekawa, *Phys. Rev. B* **83**, 094410 (2011).
- 24) E. C. Ahn, *npj 2D Mater. Appl.* **4**, 17 (2020).
- 25) J. F. Sierra, J. Fabian, R. K. Kawakami, S. Roche, and S. O. Valenzuela, *Nat. Nanotechnol.* **16**, 856 (2021).
- 26) S. Lee, W. Lee, T. Kikkawa, C. T. Le, M. Kang, G. Kim, A. D. Nguyen, Y. S. Kim, N. Park, and E. Saitoh, *Adv. Funct. Mater.* **30**, 2003192 (2020).
- 27) N. Wada et al., *Adv. Funct. Mater.* **32**, 2203602 (2022).
- 28) H. Terrones et al., *Sci. Rep.* **4**, 4215 (2014).
- 29) S. Daimon, K. Uchida, N. Ujii, Y. Hattori, R. Tsuboi, and E. Saitoh, *Appl. Phys. Express* **13**, 103001 (2020).
- 30) A. Takahagi, T. Hirai, R. Iguchi, K. Nakagawara, H. Nagano, and K. Uchida, *Appl. Phys. Express* **15**, 063002 (2022).
- 31) T. Yamazaki, R. Iguchi, H. Nagano, and K. Uchida, *Jpn. J. Appl. Phys.* **59**, 050901 (2020).
- 32) Z. Y. Zhu, Y. C. Cheng, and U. Schwingenschlögl, *Phys. Rev. B* **84**, 153402 (2011).
- 33) K. Kośmider, J. W. González, and J. Fernández-Rossier, *Phys. Rev. B* **88**, 245436 (2013).
- 34) G. Dastgeer, M. A. Shehzad, and J. Eom, *ACS Appl. Mater. Interfaces* **11**, 48533 (2019).
- 35) A. Allain, J. Kang, K. Banerjee, and A. Kis, *Nat. Mater.* **14**, 1195 (2015).
- 36) J. Kang, D. Sarkar, W. Liu, D. Jena, and K. Banerjee, *International Electron Devices Meeting*, 2012, p. 17.4.1.
- 37) Z. H. Ni, H. M. Wang, Y. Ma, J. Kasim, Y. H. Wu, and Z. X. Shen, *ACS Nano* **2**, 1033 (2008).
- 38) X. P. Qiu, Y. J. Shin, J. Niu, N. Kulothungasagaran, G. Kalon, C. Qiu, T. Yu, and H. Yang, *AIP Adv.* **2**, 032121 (2012).
- 39) J. Seo, I. Sohn, and H. Kim, *ACS Mater. Lett.* **7**, 3190 (2025).
- 40) R. Nakajima et al., *ACS Omega* **10**, 42973 (2025).
- 41) K. Gupta, R. J. H. Wesselink, R. Liu, Z. Yuan, and P. J. Kelly, *Phys. Rev. Lett.* **124**, 087702 (2020).
- 42) L. Liu, Y. Li, Y. Liu, T. Feng, J. Xu, X. R. Wang, D. Wu, P. Gao, and J. Li, *Phys. Rev. B* **102**, 014411 (2020).